Complex Heavy-Quark Potential at Finite Temperature from Lattice QCD

Alexander Rothkopf,[1,2] Tetsuo Hatsuda,[1,3] and Shoichi Sasaki[1]

[1]*Department of Physics, The University of Tokyo, Tokyo 113-0031, Japan*
[2]*Fakultät für Physik, Universität Bielefeld, D-33615 Bielefeld, Germany*
[3]*Theoretical Research Division, Nishina Center, RIKEN, Saitama 351-0198, Japan*

(Received 15 August 2011; published 18 April 2012)

We calculate for the first time the complex potential between a heavy quark and antiquark at finite temperature across the deconfinement transition in lattice QCD. The real and imaginary part of the potential at each separation distance r is obtained from the spectral function of the thermal Wilson loop. We confirm the existence of an imaginary part above the critical temperature T_C, which grows as a function of r and underscores the importance of collisions with the gluonic environment for the melting of heavy quarkonia in the quark-gluon plasma.

DOI: 10.1103/PhysRevLett.108.162001 PACS numbers: 12.38.Gc, 03.65.Ge, 12.38.Mh, 14.40.Pq

Heavy-quark bound states ($Q\bar{Q}$) are essential tools in the experimental and theoretical investigation of the high temperature state of QCD matter, the quark-gluon plasma (QGP) [1]. In particular, the suppression of heavy quarkonia such as J/ψ (the ground state of $c\bar{c}$ in the vector channel) in relativistic heavy-ion collision experiments at the Relativistic Heavy Ion Collider [2] and at the Large Hadron Collider [3] provides us with an intriguing signal of the QGP.

In order to extract the physics of the QGP from heavy quarkonia, an intuitive as well as quantitative understanding of the involved physics is necessary: In the classic approach of using a Schrödinger equation with a phenomenological $Q\bar{Q}$ potential, Debye screening of color charges is responsible for the melting of $Q\bar{Q}$ bound states above the deconfinement temperature T_C [4]. A perturbative evaluation of the thermal Wilson loop using the hard-thermal-loop resummation technique shows that the static potential at high temperature has an imaginary part induced by Landau damping [5,6]. An approach based on heavy-quark effective field theory at finite temperature indicates an additional contribution to the imaginary part of the static potential [7]. In addition, lattice QCD simulations of the spectral function of charmonia at finite temperature show that J/ψ may survive even up to $1.5T_C$ [8]. However, the connection among the different approaches is not yet clearly understood.

The main purpose of this Letter is to unify the approach based on the nonrelativistic Schrödinger equation and that based on a spectral decomposition of the $Q\bar{Q}$ correlator. Utilizing lattice QCD simulations of the medium surrounding the $Q\bar{Q}$, we extract a nonperturbative potential at *any temperature*, especially in the phenomenologically important and hitherto inaccessible region around T_C.

The starting point for deriving the effective Schrödinger equation at finite T is the real-time forward $Q\bar{Q}$ correlator ($t > 0$) [5]

$$D^{>}(\mathbf{r}, t) = \langle M(\mathbf{x}, \mathbf{y}, t) M^{\dagger}(\mathbf{x}, \mathbf{y}, 0) \rangle, \tag{1}$$

where $M(\mathbf{x}, \mathbf{y}, t) = \bar{Q}(\mathbf{x}, t) \gamma U[\mathbf{x}, \mathbf{y}] Q(\mathbf{y}, t)$ with γ denoting gamma matrices ($\gamma = \gamma^{\mu}$ for J/ψ) and $U[\mathbf{x}, \mathbf{y}]$ being a straight Wilson line connecting $(\mathbf{x}, t)$ and $(\mathbf{y}, t)$. The relative coordinate is defined as $\mathbf{r} = \mathbf{x} - \mathbf{y}$. The angular brackets imply the thermal average. In the nonrelativistic limit, where the heavy-quark mass m_Q is much larger than any other scale of the system, one may rewrite Eq. (1) in terms of a path integral over the positions and momenta of the heavy quarks:

$$D^{>}_{\mathrm{NR}}(\mathbf{r}, t) \propto \int \mathcal{D}[\mathbf{z}_1, \mathbf{z}_2, \mathbf{p}_1, \mathbf{p}_2] \times \exp\left[i \int_0^t ds \sum_{j=1,2} \left(\mathbf{p}_j(s) \dot{\mathbf{z}}_j(s) - \frac{\mathbf{p}_j^2(s)}{2m_Q} \right) \right] W_{\Gamma} \tag{2}$$

with the Wilson loop $W_{\Gamma} = \langle \exp[-ig \int_{\Gamma} dx_{\mu} A^{\mu}(x)] \rangle$. Here Γ denotes a closed loop in Minkowski space-time, defined by the path of the quark and antiquark. This formula is a finite temperature generalization of the result in Ref. [9] and is valid up to $O(1/m_Q)$.

From here on, we focus on the leading part of the potential, obtained in the heavy-quark limit $m_Q \to \infty$. In this case, it is enough to consider a rectangular path for the Wilson loop $W_{\Gamma} \to W_{\square}(r = |\mathbf{z}_1 - \mathbf{z}_2|, t)$ with a Fourier decomposition:

$$W_{\square}(r, t) = \int_{-\infty}^{+\infty} d\omega e^{-i\omega t} \rho_{\square}(r, \omega). \tag{3}$$

Equation (1) for $m_Q \to \infty$ also has a spectral decomposition composed of three parts, ρ_{loop}, ρ_{staple}, and ρ_{handle}: One can show that $\rho_{\square}(r, \omega)$ in Eq. (3) corresponds to ρ_{loop} and is positive semidefinite for all r and ω [10].

Through Eq. (3), we are led to the following nonperturbative definition of the in-medium potential:

$$\frac{i\partial_t W_\square(r,t)}{W_\square(r,t)} = \frac{\int d\omega \omega e^{-i\omega t}\rho_\square(r,\omega)}{\int d\omega e^{-i\omega t}\rho_\square(r,\omega)} \equiv V_\square(r,t). \quad (4)$$

Indeed, the solution of Eq. (4) yields the transfer matrix compatible relation $W_\square(r,t) = \exp[-i\int_0^t V_\square(r,s)ds]$ and thus leads to an in-medium Schrödinger equation

$$i\partial_t D^>_{\rm NR}(\mathbf{r},t) = \left(-\frac{\nabla_r^2}{m_Q} + V_\square(r,t)\right) D^>_{\rm NR}(\mathbf{r},t). \quad (5)$$

In the following, we study the peaks of the spectral function in Eq. (4) around $\omega = 0$, since it is the physics at late times t that determines the potential. Based on Eq. (4), the real part of the potential is thus given by the peak position, whereas the imaginary part is related to the peak width: For example, if $\rho_\square(r,\omega)$ exhibits a Breit-Wigner peak with position $\omega_0(r)$ and width $\Gamma_0(r)$, we obtain $V_\square(r,t) \to V^{(\rm BW)}(r) = \omega_0(r) + i\Gamma_0(r)$, while if it contains a single Gaussian peak, we have $V_\square(r,t) \to V^{(\rm G)}(r,t) = \omega_0(r) + i\Gamma_0^2(r)t$.

A nonperturbative method to determine $\rho_\square(r,\omega)$ and hence $V_\square(r,t)$ for all T is based on lattice QCD simulations. We first make an analytic continuation of Eq. (3) to imaginary time and connect the Euclidean thermal Wilson loop to the spectral function through the Laplace transform: $W^{\rm E}_\square(r,\tau) = \int d\omega e^{-\omega\tau}\rho_\square(r,\omega)$. This quantity is purely real and not symmetric under the reflection $\tau \leftrightarrow \beta - \tau$ by definition. As shown in Ref. [10], $\rho_\square(r,\omega)$ in a finite volume allows for a spectral decomposition in terms of delta-function peaks:

$$\rho_\square(r,\omega) = \sum_{n,n'} P_n(T)|A_{n,n'}(r)|^2 \delta(\omega - E^{Q\bar{Q}}_{n'}(r) + E_n). \quad (6)$$

Here E_n is the energy eigenvalue of a state $|n\rangle$ without $Q\bar{Q}$, while $E^{Q\bar{Q}}_{n'}(r)$ is the eigenvalue (relative to $2m_Q$) of a state $|n';r\rangle$ including a $Q\bar{Q}$ separated by a distance r. The matrix element and the Boltzmann factor are defined as $A_{nn'}(r) \equiv \sum_{\mathbf{y}}\langle n|M(\mathbf{y}+\mathbf{r},\mathbf{y},t=0)|n'\rangle$ and $P_n(T) \equiv e^{-E_n/T}/[\sum_n e^{-E_n/T}]$, respectively. The peak positions of Eq. (6) do not depend on T [since E_n and $E^{Q\bar{Q}}_{n'}(r)$ are T-independent], while the pole residues $P_n(T)|A_{n,n'}(r)|^2$ depend on T due to the Boltzmann factor. The various possible combinations of n' and n in $\rho_\square(r,\omega)$ at finite T lead to a number of peaks as large as $N \times N$, if $\rho_\square(r,\omega)$ at $T = 0$ has N peaks.

The position and width of a physical resonance in an *infinite* volume are obtained from the *envelope* of a bunch of delta-function peaks in Eq. (6). A suitable technique to extract such envelopes from lattice QCD data of $W^{\rm E}_\square(r,\tau)$ is the maximum entropy method (MEM) [11]. In this Letter, we utilize a high precision MEM with an extended search space developed by one of the present authors [12]. By separating the size of the search space from the number of data points, it allows a consistent comparison of spectra even if the temporal extent of the underlying lattice is changed.

The stability of the position and width of the resonance reconstructed by the MEM can be checked through changing the amplitude of the prior and by increasing the number of temporal data points [11]. In addition, the effect of a discrete lattice spectrum on the position and width of the resonance can be checked by controlling the number of peaks and their relative separation under the variation of the lattice spacing a and the lattice size L (see, e.g., [13] for the variation of a).

We perform quenched lattice QCD simulations of $W^{\rm E}_\square(r,\tau)$ by using the simple plaquette gauge action on an anisotropic $20^3 \times N_\tau$ lattice. The anisotropy ratio between the spatial and temporal lattice spacing is taken to be $\xi \equiv a_\sigma/a_\tau = 4$. We fix a_σ to be 0.097 fm ($\beta = 6.1$) and adopt the temporal lattice sizes $N_\tau = 36, 24, 12$ which correspond to temperatures $T/T_C = 0.78, 1.17, 2.33$ with $T_C \simeq 290$ MeV [14]. Our spatial lattice size $L \sim 2$ fm can accommodate the characteristic J/ψ scale of $r_{J/\psi} \sim 0.5$ fm. After collecting the lattice data, we carry out the MEM over a frequency interval $I_\omega = [\omega_{\rm min}, \omega_{\rm max}]$ of $N_\omega = 1500$ points. Our choice corresponds to $I_\omega \simeq [-21\ {\rm GeV}, 42\ {\rm GeV}]$ at $N_\tau = 24$. We use a prior distribution of the form $m(\omega) = \frac{1}{\omega+\omega_0}$, motivated by the canonical dimension of $\rho_\square(r,\omega)$. The parameter $\omega_0(>0)$ is fixed by setting the amplitude $m_0 = m(\omega_{\rm min})$ at the smallest frequency in I_ω.

In Fig. 1 (left), we plot typical Wilson-loop data as a function of τ for various distances r at $T = 1.17T_C$. Spectral functions obtained by the MEM at $r = a_\sigma \simeq 0.1$ fm and $r = 4a_\sigma \simeq 0.39$ fm are plotted in Fig. 1 (right). The falloff of $W^{\rm E}_\square(r,\tau)$ for small and intermediate values of τ in the left figure corresponds to the peaks located in the $\omega > 0$ region seen in the right figure: They arise from gluonic interactions between the temporal Wilson lines. The upward trend of $W^{\rm E}_\square(\tau,r)$ around $\tau = \beta$, on the other hand, is induced by extremely small structures located in the $\omega < 0$ region: These arise from short distance gluon interactions connecting the spatial Wilson lines across the compactified temporal axis. Although the spectral function in the negative ω region is important for reproducing $W^{\rm E}_\square(r,\tau \sim \beta)$ due to its exponential "enhancement" by the Laplace transform, its effect on $V_\square(r,t)$ in Eq. (4) is negligible due to its extremely small residue.

The real and imaginary parts of the potential are obtained from fitting the lowest lying peak with a Breit-Wigner and Gaussian shape. The identical results for position and width are shown in Fig. 2 (left) and (right), respectively. The error bars are obtained from the variance in the peak structure between different choices for the amplitude of the prior distribution. The interval of $10^{-2} \geq m_0 \geq 10^{-6}$ is chosen to span as many orders without introducing numerical instabilities in the minimization process. We have checked that the standard MEM error,

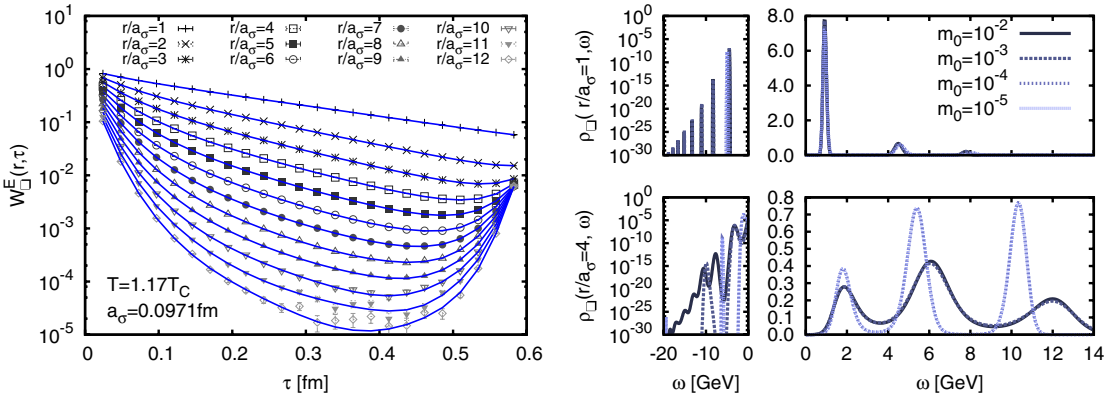

FIG. 1 (color online). (Left) Lattice data for the Euclidean thermal Wilson loop as a function of the imaginary time τ at $T/T_C = 1.17$. The solid lines show the results obtained after the MEM reconstruction of the spectral function. (Right) Spectral functions and their prior dependence obtained by the MEM with the thermal Wilson-loop data at $r/a_\sigma = 1, 4$. Positive ω regions and negative ω regions are plotted separately with a different vertical scale.

estimated from the stability of the spectral function given m_0 [11], is much smaller than the error from the variation of m_0.

$T = 0.78T_C$: Re$[V_\square(r)]$ denoted by the filled squares in Fig. 2 (left) is found to show a linearly rising potential at long distances, a result consistent with quark confinement below T_C. To study the short distance behavior of the potential, we have also carried out simulations with a 2.5 times smaller lattice spacing ($\beta = 7$, $\xi = 4$, $a_\sigma = 0.039$ fm, $20^3 \times 96$) at the same T/T_C; the resulting Re$[V_\square(r)]$ can be fitted well by a Coulomb + linear potential [15]. Furthermore, our results agree with the color-singlet free energies $F^1(r)$ in the Coulomb gauge (solid black line in the left panel) at all measured distances r. Note that $\Gamma_\square(r)$ appears to be small and is consistent with zero within the statistical and systematic errors; see the filled squares in Fig. 2 (right).

$T = 1.12T_C$: At this temperature, Re$[V_\square(r)]$ has apparently frozen at around the same strength found at $T = 0.78T_C$, as shown by the filled circles in the left panel. This is in contrast to the behavior of $F^1(r)$ at the same T (the long dashed curve in the left panel) which exhibits a significant thermal screening. As for $\Gamma_\square(r)$, there is a tendency to develop a nonzero value, which grows as r increases; see the filled circles in the right panel.

$T = 2.33T_C$: At the highest available temperature, Re$[V_\square(r)]$ and $\Gamma_\square(r)$ exhibit a strong rise as a function of r, shown by the filled triangles. To test the effects of a small number of temporal data points N_τ [11] and also whether the discrete lattice spectrum [13] might blur the MEM image and thus might lead to an artificial broad peak, we compare the results of ($\beta = 6.1$, $a_\sigma = 0.097$ fm, $20^3 \times 12$) and those of ($\beta = 7$, $\xi = 4$, $a_\sigma = 0.039$ fm, $20^3 \times 32$): The latter has more temporal data points; hence, it has finer (coarser) resolution at low (high) frequency. The results shown by solid diamonds in Fig. 2 (left) and (right) are consistent with the solid triangles. This cross-check indicates that the width broadening

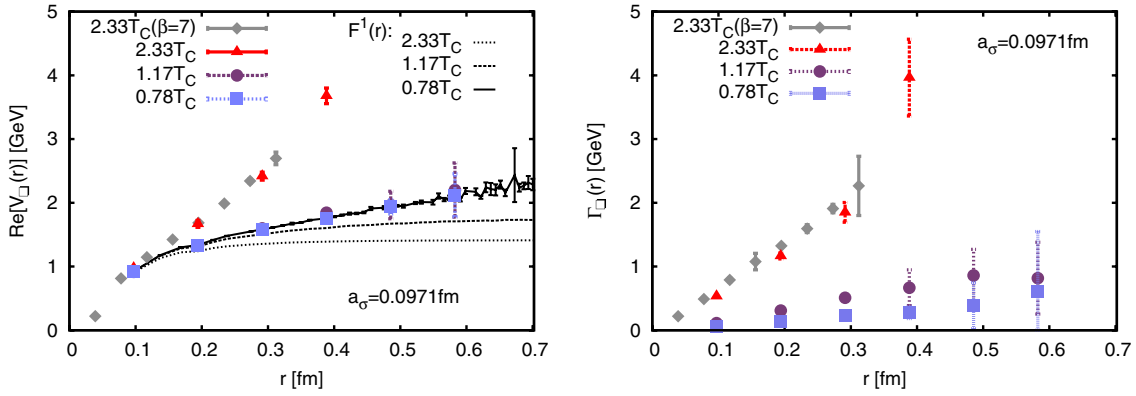

FIG. 2 (color online). (Left) The real part of the in-medium heavy-quark potential for three different temperatures across T_C with $a_\sigma = 0.0971$ fm (solid squares, circles, and triangles). Solid and dashed lines are the color-singlet free energies $F^1(r)$ in the Coulomb gauge at corresponding temperatures. The result for the finer lattice ($a_\sigma = 0.039$ fm at $T/T_C = 2.33$) is also shown for comparison (solid diamonds). (Right) The imaginary part of the potential, obtained from the width of the lowest lying peak of the spectral function. The same symbols are used as the left figure.

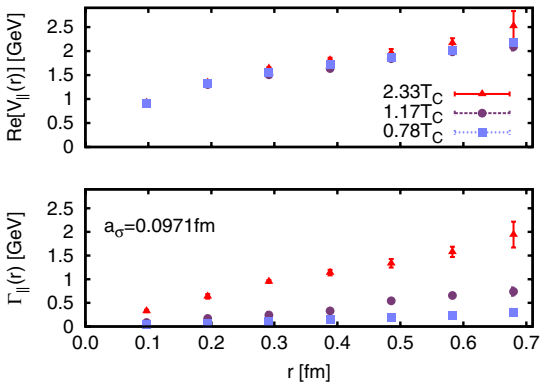

FIG. 3 (color online). The real part (upper panel) and the imaginary part (lower panel) of the potential obtained from the Wilson lines $W_{||}^{\mathrm{E}}$.

observed from the MEM is a physical effect [16]. We need, however, further systematic studies to confirm this point by changing N_τ, a, and L independently.

Although we construct our potential by starting from the mesonic operator $M(\mathbf{x}, \mathbf{y}, t)$ with a straight Wilson line in Eq. (1), one has the freedom to choose the operator M differently and, hence, the forward correlator $D^>$ and the potential V. On the other hand, observable quantities, such as the dilepton emission rate, must be independent of such differences [17]. Therefore, there must be a trade-off between the real and the imaginary part of the potential to leave the observables unchanged. To study this point, we consider an operator M with $U[\mathbf{x}, \mathbf{y}] = 1$ in the Coulomb gauge. In this case, we have "Wilson lines" without the spatial link $W_{||}(r, t)$. In Fig. 3, we show the real and imaginary parts of the potential ($V_{||}$) obtained from $W_{||}^{\mathrm{E}}(r, \tau)$. In the confinement phase below T_C, $V_{||}$ and $V_\square$ agree quite well. On the other hand, in the deconfinement phase, both $\mathrm{Re}[V_{||}(r)]$ and $\Gamma_{||}(r)$ exhibit a less pronounced rise in r. We observe that a weaker real part is accompanied by a weaker spectral width, which could be a sign of the trade-off mentioned above. This mechanism has to be made quantitative in future studies by solving the time-dependent Schrödinger equation for an initial $Q\bar{Q}$ wave packet entering the QGP.

We have presented a nonperturbative derivation of the Schrödinger equation for heavy quarkonia and a first evaluation of the corresponding *complex* in-medium potential, based on quenched lattice QCD. Our numerical results show that, even though the potential agrees with the color-singlet free energies below the phase transition, the correct physics above T_C can be obtained only if the real and imaginary parts are taken into account together. The temperature-insensitive real part around T_C suggests furthermore that the growth of the imaginary part, i.e., an increasing number of collisions with the medium, may play a more important role to destabilize $Q\bar{Q}$ than the screening effects [18]. We have also discussed a possible mechanism to obtain the relevant physics independent of a particular choice of the underlying operator by balancing the real and imaginary parts. Our complex potential opens up new possibilities to study the dynamics of the QGP transition by providing first-principles input to nonrelativistic real-time simulations, going beyond both models and perturbation theory.

Our ongoing work aims at full QCD simulations with dynamical fermions, since these additional degrees of freedom may affect both the real and imaginary parts of the complex potential substantially. In addition, larger and finer lattices are needed in order to assess the relative significance of Debye screening vs the collisional effects from short distance to long distance in more detail.

The authors thank T. Matsui, H. Satz, and M. Laine for stimulating discussions, N. Brambilla and Y. Burnier for insight into potential nonrelativistic QCD, and Y. Maezawa for his support with the lattice setup. A. R. acknowledges support through from MEXT and the Young Researchers Initiative of the supercomputing center at The University of Tokyo. A. R. and T. H. were partially supported by Grant-in-Aid of MEXT No. 22340052.

[1] S. Sarkar, H. Satz, and B. Sinha, Lect. Notes Phys. **785**, 1 (2010).
[2] A. Adare *et al.*, Phys. Rev. C **84**, 054912 (2011).
[3] G. Aad *et al.*, Phys. Lett. B **697**, 294 (2011).
[4] T. Matsui and H. Satz, Phys. Lett. B **178**, 416 (1986).
[5] M. Laine, O. Philipsen, M. Tassler, and P. Romatschke, J. High Energy Phys. 03 (2007) 054; M. Laine, J. High Energy Phys. 05 (2007) 028.
[6] A. Beraudo, J. P. Blaizot, and C. Ratti, Nucl. Phys. **A806**, 312 (2008).
[7] N. Brambilla, J. Ghiglieri, A. Vairo, and P. Petreczky, Phys. Rev. D **78**, 014017 (2008).
[8] M. Asakawa and T. Hatsuda, Phys. Rev. Lett. **92**, 012001 (2004); T. Umeda, K. Nomura, and H. Matsufuru, Eur. Phys. J. C **39**, 9 (2004); S. Datta, F. Karsch, P. Petreczky, and I. Wetzorke, Phys. Rev. D **69**, 094507 (2004); A. Jakovac, P. Petreczky, K. Petrov, and A. Velytsky, Phys. Rev. D **75**, 014506 (2007); G. Aarts, C. Allton, M. B. Oktay, M. Peardon, and J.-I. Skullerud, Phys. Rev. D **76**, 094513 (2007); H.-T. Ding *et al.*, Proc. Sci., LAT2010 (**2010**) 180; H. Ohno *et al.* (WHOT-QCD Collaboration), Phys. Rev. D **84**, 094504 (2011).
[9] A. Barchielli, E. Montaldi, and G. M. Prosperi, Nucl. Phys. **B296**, 625 (1988); A. Barchielli, N. Brambilla, and G. M. Prosperi, Nuovo Cimento Soc. Ital. Fis. A **103**, 59 (1990).
[10] A. Rothkopf, T. Hatsuda, and S. Sasaki, Proc. Sci., LAT2009 (**2009**) 162.
[11] M. Asakawa, Y. Nakahara, and T. Hatsuda, Prog. Part. Nucl. Phys. **46**, 459 (2001).
[12] A. Rothkopf (to be published, source code available at http://www.scicode.org/ExtMEM).
[13] T. Yamazaki *et al.* (CP-PACS Collaboration), Phys. Rev. D **65**, 014501 (2001).

[14] H. Matsufuru, T. Onogi, and T. Umeda, Phys. Rev. D **64**, 114503 (2001).

[15] Since $W_{\square}(r, \tau)$ at low T is clearly dominated by a single exponential falloff, we used naive exponential fitting for $\beta = 7$ in the determination of $V_{\square}(r)$ at small r.

[16] In our preliminary result at $T = 2.33T_C$ reported in Ref. [10], we could not identify the strong rise of $V_{\square}(r)$ due to unstable exponential fitting of the data with small statistics.

[17] Y. Burnier, M. Laine, and M. Vepsalainen, J. High Energy Phys. 01 (2008) 043.

[18] K. Morita and S. H. Lee, Phys. Rev. Lett. **100**, 022301 (2008); P. Gubler, K. Morita, and M. Oka, Phys. Rev. Lett. **107**, 092003 (2011).